WATER RESOURCES RESEARCH, VOL. 49, 6731–6743, doi:10.1002/wrcr.20537, 2013

The 2010/2011 snow season in California's Sierra Nevada: Role of atmospheric rivers and modes of large-scale variability

Bin Guan,[1,2] Noah P. Molotch,[1,3] Duane E. Waliser,[1] Eric J. Fetzer,[1] and Paul J. Neiman[4]

Received 4 January 2013; revised 15 September 2013; accepted 16 September 2013; published 17 October 2013.

[1] The anomalously snowy winter season of 2010/2011 in the Sierra Nevada is analyzed in terms of snow water equivalent (SWE) anomalies and the role of atmospheric rivers (ARs)—narrow channels of enhanced meridional water vapor transport between the tropics and extratropics. Mean April 1 SWE was 0.44 m (56%) above normal averaged over 100 snow sensors. AR occurrence was anomalously high during the period, with 20 AR dates during the season and 14 in the month of December 2010, compared to the mean occurrence of nine dates per season. Fifteen out of the 20 AR dates were associated with the negative phases of the Arctic Oscillation (AO) and the Pacific-North American (PNA) teleconnection pattern. Analysis of all winter ARs in California during water years 1998–2011 indicates more ARs occur during the negative phase of AO and PNA, with the increase between positive and negative phases being ~90% for AO, and ~50% for PNA. The circulation pattern associated with concurrent negative phases of AO and PNA, characterized by cyclonic anomalies centered northwest of California, provides a favorable dynamical condition for ARs. The analysis suggests that the massive Sierra Nevada snowpack during the 2010/2011 winter season is primarily related to anomalously high frequency of ARs favored by the joint phasing of −AO and −PNA, and that a secondary contribution is from increased snow accumulation during these ARs favored by colder air temperatures associated with −AO, −PNA, and La Niña.

Citation: Guan, B., N. P. Molotch, D. E. Waliser, E. J. Fetzer, and P. J. Neiman (2013), The 2010/2011 snow season in California's Sierra Nevada: Role of atmospheric rivers and modes of large-scale variability, *Water Resour. Res.*, *49*, 6731–6743, doi:10.1002/wrcr.20537.

1. Introduction

[2] The 2010/2011 winter season in the Sierra Nevada, California, had a large number of winter storms associated with atmospheric river (AR) landfalls, and a massive April 1 snowpack with near-record levels of snow water equivalent (SWE) at many locations. This happened in a period with large anomalies in the Northern Hemisphere atmosphere, such as large amplitudes of the Arctic Oscillation (AO) and the Pacific North American teleconnection pattern (PNA), as well as strong La Niña conditions with mean sea surface temperature (SST) anomalies in the equatorial central/eastern Pacific (the Niño3.4 region) about three times the practical La Niña threshold of −0.5 K. In the context of the observed [*Kapnick and Hall*, 2010] and projected [*Waliser et al*., 2011, 2012] decline in the Sierra Nevada snowpack, an anomalous winter of this magnitude highlights the need to understand the full range of natural climate variability in the Sierra Nevada in order to better appreciate and convey regional climate projections. Such understanding of regional climate change and natural variability is critical as the Sierra Nevada snowpack provides the main source of water in the area for agriculture, recreation, hydropower, urban supply, and downstream habitats [*Bales et al*., 2006] and strongly influences ecosystem function [*Trujillo et al*., 2012]. Meanwhile, exploration of the possible causes of the natural variability of snowpack, including related meteorological and hydrological extremes, will help to better forecast and manage water resources and floods in California and across the western US.

[3] Our focus on ARs and the Sierra Nevada snowpack stem from their importance to the regional climate, hydrology, and water resources. ARs are narrow channels of enhanced water vapor transport in the atmosphere [*Zhu and Newell*, 1994]. They are responsible for over 90% of the water vapor transport between the tropics and extratropics while occupying less than 10% of the circumference of the earth surface [*Zhu and Newell*, 1998]. The structure of ARs became directly observed and better characterized relatively recently with dedicated field campaigns and improvements in satellite remote sensing [*Ralph et al*., 2004, 2005; *Neiman et al*., 2008a]. A record of historical AR landfalls along the west coast of North America has

[1]Jet Propulsion Laboratory, California Institute of Technology, Pasadena, California, USA.
[2]Joint Institute for Regional Earth System Science and Engineering, University of California, Los Angeles, California, USA.
[3]Department of Geography and Institute for Arctic and Alpine Research, University of Colorado at Boulder, Boulder, Colorado, USA.
[4]Earth System Research Laboratory, Physical Sciences Division, NOAA, Boulder, Colorado, USA.

Corresponding author: B. Guan, Jet Propulsion Laboratory, MS 233-300, California Institute of Technology, 4800 Oak Grove Dr., Pasadena, CA 91109, USA. (bin.guan@jpl.nasa.gov)

0043-1397/13/10.1002/wrcr.20537

been created based on the improved understanding on AR structure [*Neiman et al*., 2008a]. The impacts of ARs on precipitation, stream flow, and mountain snowpack have been extensively documented, with the critical role of ARs in extreme hydrological events becoming increasingly appreciated [*Ralph et al*., 2006; *Neiman et al*., 2008a, 2008b; *Leung and Qian*, 2009; *Guan et al*., 2010; *Dettinger et al*., 2011; *Neiman et al*., 2011; *Lavers et al*., 2011, 2012; *Moore et al*., 2012; *Ralph and Dettinger*, 2012; *Kim et al*., 2013; *Neiman et al*., 2013]. On the other hand, the connection between AR activity and the large-scale ocean-atmosphere dynamics remain less explored. *Ralph et al*. [2011] discussed the role of multiscale tropical and extratropical waves in the high-impact AR landfall in the Pacific Northwest during March 2005. *Jiang and Deng* [2011] linked AR activity in the North Pacific to East Asian cold surges. *Guan et al*. [2012] showed that the largest number of high-impact AR landfalls occurred in the Sierra Nevada when enhanced convection associated with the Madden-Julian Oscillation (MJO) was located in the western Pacific compared to other phases of the MJO. *Lavers et al*. [2012] connected annual AR occurrence in Britain to the Scandinavian Pattern. These studies suggested the close connection between AR activity and several important components of the large-scale ocean-atmosphere variability.

[4] Building on these previous studies and in view of the anomalous 2010/2011 winter season in the Sierra Nevada, the current work explores the connection between AR activity and two of the most prominent modes of the Northern Hemisphere atmospheric variability, namely, the Arctic Oscillation (AO) and the Pacific-North American (PNA) teleconnection pattern, both of which were anomalously strong during the 2010/2011 winter season. The AO is characterized by sea level pressure anomalies of one sign in the Arctic area and anomalies of opposite sign in the surrounding extratropical areas [*Thompson and Wallace*, 1998]. The positive phase of AO is associated with enhanced midlatitude winds blowing consistently from the west to the east, which help keep the cold air to the Arctic region. These winds become weaker during the negative phase of AO, favoring southward excursion of cold Arctic air [*Jeong and Ho*, 2005]. The PNA is characterized by a wave train pattern with four centers of actions linking the Pacific Ocean and the North American continent. The positive phase of PNA is associated with high pressure anomalies over the tropical Pacific (in the vicinity of Hawaii) and western North America, and low pressure anomalies in the extratropical North Pacific (south of the Aleutian Islands) and southeastern North America [*Wallace and Gutzler*, 1981]. The opposite happens during the negative phase of PNA. Both the AO and the PNA have the largest variability during the cold season, with profound impacts on weather and climate. In general, less stormy weather in the western US has been linked to the positive phase of AO and PNA. For example, *McAfee and Russell* [2008] showed the positive phase of AO is followed by dry and warm springs west of the Rocky Mountains in relation to the poleward retraction of storm tracks. *Cayan* [1996] showed reduced snow accumulation over most of the western US is associated with the positive phase of PNA when the Pacific storms are diverted away from the region by the PNA-related low pressure anomalies over the extratropical North Pacific and high pressure anomalies over the western North America. As ARs account for the most extreme precipitation in the US west coast [*Ralph and Dettinger*, 2012], they are presumably favored by the negative phase of AO and PNA when the weather is in general wet and cold. The 2010/2011 winter season provides an interesting case to study and motivation for a broader climatological analysis.

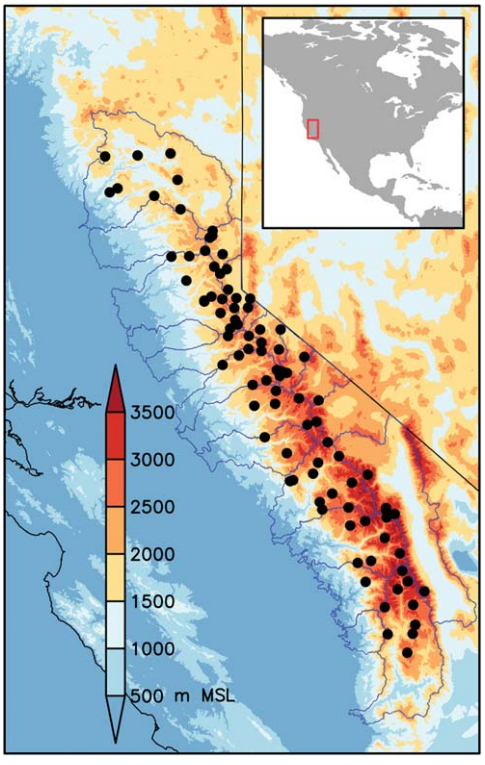

Figure 1. Elevation (m; shading) map showing the Sierra Nevada domain (20 watersheds delineated by the blue lines) and the snow sensor network (dots).

[5] The main objective of the current work is to test the above hypothesis on the connection between ARs and the phases of the AO and PNA, and if true evaluate the role of such connection in the anomalously snowy 2010/2011 winter season in the Sierra Nevada. In that context, possible role of ENSO will also be examined, given strong La Niña conditions of the season. The period of November–March is considered, which is the main period of snow accumulation in the Sierra Nevada. The analysis covers water years (WY) 1998–2011, for which Special Sensor Microwave Imager (SSM/I) and the Special Sensor Microwave Imager/Sounder (SSMIS) satellite observations of integrated water vapor (IWV) are available [e.g., *Hollinger et al*., 1990], which readily enable the detection of ARs over the adjacent Pacific Ocean.

2. Data and Methods

2.1. Snow Water Equivalent (SWE)

[6] Observed SWE from 100 snow sensor stations in the Sierra Nevada (Figure 1) is obtained from the California Data Exchange Center (http://cdec.water.ca.gov). All stations used are above 1500 m elevation. Daily observations date back to the late 1970s. This product is the primary

SWE product used for the current study given its longest period of availability. To illustrate the uncertainty in estimating the distribution of SWE at the mountain range scale, two gridded SWE products are also used, which are based on forward modeling and reconstruction, respectively. The two gridded products are assimilated SWE from the Snow Data Assimilation System (SNODAS), and a recently developed product based on the blend of snow sensor observations and snowmelt model reconstructions [*Guan et al*., 2013]. The SNODAS product is produced by the National Operational Hydrologic Remote Sensing Center (NOHRSC). Daily gridded SWE at 30 arc sec (∼1 km) resolution is available from September 30, 2003 [*National Operational Hydrologic Remote Sensing Center*, 2004], which assimilates snow observations from ground-based, airborne, and satellite platforms [*Carroll et al*., 2001]. The new blended SWE product is produced as follows: First, daily historical SWE is reconstructed using an energy-balanced, spatially distributed snowmelt model [*Molotch*, 2009; *Jepsen et al*., 2012]. Second, reconstructed SWE is then corrected for errors by calculating the residuals at snow sensor stations, which are distributed to each model pixel based on the inverse of distance-squared. From these steps, daily blended SWE at 15 arc sec (∼500 m) resolution has been produced for the period of 2000–2012. The accuracy of this product relative to SNODAS is evaluated using thousands of field observations in the Sierra Nevada. The root-mean-square (RMS) error of the blended and SNODAS SWE is 0.21 and 0.25 m, respectively, based on the validation analysis reported in *Guan et al*. [2013].

2.2. Atmospheric Rivers (ARs)

[7] ARs are defined by *Ralph et al*. [2004] as water vapor structures longer than 2000 km in length, shorter than 1000 km in width, and with greater than 2 cm IWV. In this definition, IWV is used as a proxy for water vapor transport based on the close correspondence between such filamentary IWV structure and enhanced water vapor transport. This definition is used by *Neiman et al*. [2008a] to create the satellite-based record of landfalling ARs onto the west coast of North America, which gives the list of dates when a 2 cm IWV "river" intersects the coast of California (south of 41°N) or the Pacific Northwest (north of 41°N) as observed by the SSM/I and the SSMIS. This record now covers the period of WY1998–2011.

2.3. Climate Indices

[8] Daily indices of AO and PNA calculated by the National Oceanic and Atmospheric Administration/Climate Prediction Center (NOAA/CPC) are used to characterize the large-scale atmospheric circulation. In their calculations, the loading patterns of AO and PNA (as described in section 1) were first extracted from Empirical Orthogonal Function (EOF) analysis of the 1000 hPa (for AO) or 500 hPa (for PNA) geopotential height anomalies poleward of 20°N. The AO and PNA indices were then calculated by projecting the daily 1000 hPa or 500 hPa geopotential height anomalies to their respective loading patterns (http://www.cpc.noaa.gov/products/). The Niño3.4 index, defined as mean SST anomalies in the equatorial central/eastern Pacific (170–120°W, 5°S–5°N) is used as an indicator of El Niño/Southern Oscillation (ENSO) conditions [*Trenberth*, 1997]. Daily values of the Niño3.4 index are calculated from the 0.25° resolution NOAA optimum interpolation SST [*Reynolds et al*., 2007], with a 5 month running mean applied.

2.4. Atmospheric Circulation and Water Vapor

[9] Daily geopotential height, wind, and specific humidity at 2.5° horizontal resolution are from the National Centers for Environmental Prediction (NCEP)/National Center for Atmospheric Research (NCAR) reanalysis [*Kalnay et al*., 1996]. Integrated water vapor transport (IVT) is derived from the reanalysis wind and specific humidity at eight vertical levels between 1000 and 300 hPa. The reanalysis data are available from 1948. The same data set was used in the calculation of the AO and PNA indices described above. For the more recent period (WY2003-onward), daily IWV at 1° horizontal resolution is obtained from twice daily Atmospheric Infrared Sounder (AIRS) version 5 level 3 satellite retrievals [*Chahine et al*., 2006], and used in addition to the reanalysis IVT. The higher resolution AIRS IWV is used in lieu of the reanalysis IWV for a better depiction of the water vapor gradients across the AR and because the SSMI and SSMIS water vapor data are not available over land. The AIRS IWV also provides an independent depiction of the AR structure in addition to the reanalysis IVT since AIRS data are not assimilated in the NCEP/NCAR reanalysis.

3. Results

3.1. SWE Anomalies

[10] All three SWE data sets analyzed show predominantly positive SWE anomalies on April 1, 2011 in the Sierra Nevada (Figure 2, top); anomalies are relative to the 2004–2011 mean April 1 SWE of each product (Figure 2, bottom). Negative anomalies in SNODAS and blended SWE are limited to lower elevation areas with an intermittent winter snowpack; the limited extent of these areas makes them insignificant with regard to the analyses presented herein. The domain mean anomalies are 0.44 m (56%), 0.35 m (88%), and 0.32 m (59%) above the 2004–2011 climatology based on snow sensor, SNODAS, and blended SWE, respectively. Larger differences are seen in minimum and maximum anomalies of the three products. The difference between snow sensor SWE and the other two products is largely attributable to the representative spatial scales [*Molotch and Bales*, 2005, 2006]. Snow sensor SWE is essentially a point value, while SNODAS and blended SWE represent the mean SWE over each model pixel (∼1 km for SNODAS, and ∼500 m for blended SWE). Also, the snow sensor network has a better coverage of the middle elevations than the lower and higher elevations. The difference between the two gridded products could be explained by the different approaches (forward modeling versus reconstruction), model physics, and model input. Detailed comparison of the three SWE products can be found in *Guan et al*. [2013]. With these notes on product differences and uncertainties, snow sensor SWE is used in the subsequent analysis since it is the only product that covers the entire period of the AR record.

3.2. Atmospheric Rivers and Climate Conditions

[11] Contribution of ARs to the total seasonal snow accumulation in the Sierra Nevada is shown in Figure 3 for

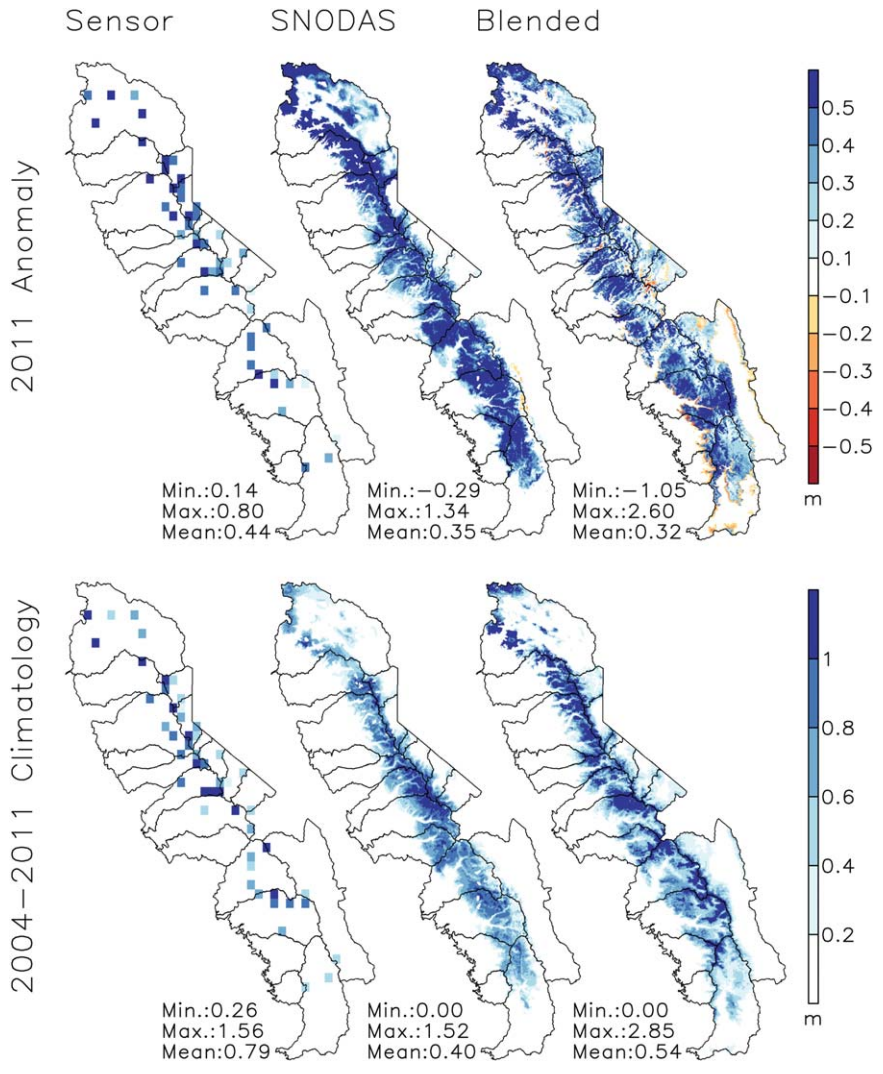

Figure 2. (top) SWE anomalies (m) on 1 April 2011 relative to (bottom) the mean April 1 SWE (m) over the period of 2004–2011 based on three SWE products: (left) snow sensor SWE, (center) SNODAS SWE, and (right) blended SWE.

each winter season during WY1998–2011. AR-related SWE accumulation is calculated as the change between 1 day before and 1 day after an AR date (or a multiday period when several AR dates occur consecutively), and non-AR SWE is taken as the difference between the seasonal total SWE accumulation and the AR contribution. Similar calculations were done in *Guan et al*. [2010] for the period of WY2004–2010 based on SNODAS SWE. On average, nine AR dates per winter during WY1998–2011 contributed 37% of the total snow accumulation based on snow sensor SWE. WY2011 clearly stands out with the largest seasonal snow accumulation, largest number of ARs, and largest AR-related snow accumulation over the analysis period. AR frequency was double the 14 year mean. Also, the AR contribution to SWE exceeded 50%, which only happened one other time during the analysis period. Non-AR winter storms on average produce less intense but more frequent SWE accumulation in the Sierra Nevada [*Guan et al*., 2012]. To compare with ARs, we define non-AR wet days as the days not meeting the AR criteria in *Ralph et al*. [2004] but with daily SWE increase greater than 0.1 mm [e.g., *Kim et al*., 2013]. Unlike ARs, the number of non-AR wet days and non-AR contribution to SWE were near normal (i.e., close to the 14 year mean) during WY2011. The unusualness of the number of ARs in WY2011 is further demonstrated in Figure 4, which shows the statistical distribution of the monthly AR occurrence (number of AR dates per month) for each calendar month during WY1998–2011. Mean AR occurrence is the largest in December, which also has the largest interannual variability. A total of 14 AR dates occurred during December 2010, placing the month well beyond the normal range (i.e., 1.5 interquartile range above the third quartile).

[12] The increased AR occurrence in WY2011, especially in December 2010, needs to be understood in the context of the large-scale atmospheric circulation conditions. Daily time series of the AO and PNA indices during November–March, WY2011 are shown in Figure 5, along with the mean daily SWE changes (ΔSWE) in the Sierra Nevada. Dates with AR landfalls in California are also

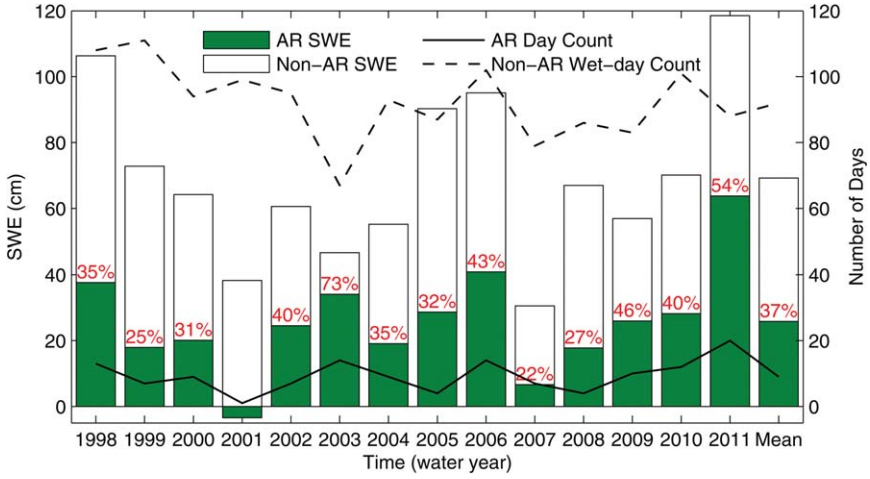

Figure 3. Snow sensor estimates of SWE (cm) over the Sierra Nevada associated with ARs compared to the total seasonal (November–March) accumulation (bars). Percentage contribution of ARs to the seasonal snow accumulation is indicated (red numerals). Also shown is the number of AR dates (solid line) and non-AR wet dates (dashed line) each season. The multiyear mean is shown with the rightmost bar in each plot. AR percentage contribution is not shown for WY2001 when the season's sole AR occurred late in the cool season and reduced the SWE.

indicated. The AO and the PNA were both in positive phase at the beginning of November. The PNA changed to its negative phase in mid-November, followed closely by the AO by a few days. Both then stayed in negative phase for several weeks. The AO index was below one negative standard deviation around late November and from mid-December to mid-January. The PNA index was at or below one negative standard deviation from mid-November to late December. Both indices were generally less than zero during the majority of December, and ∼2–3 standard deviations below zero during 18–22 December.

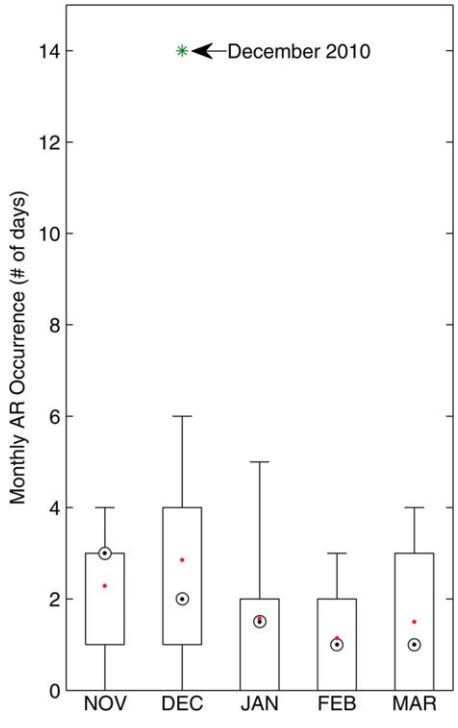

Figure 4. Box-whisker plot of monthly AR occurrence (number of AR days in a calendar month) in California during the winter months (November–March) of WY1998–2011. Also shown are medians (target signs), means (red dots), and the statistical outlier (i.e., greater than 1.5 interquartile range above the third quartile; green asterisk for December 2010).

[13] Out of the 20 AR dates of the season, 15 (i.e., 14 in December and 1 in mid-November) occurred when the AO and the PNA were both in negative phases (denoted as −AO and −PNA). In particular, five AR dates occurred consecutively during 18–22 December, accompanied by strongly negative AO and PNA. Figure 5 suggests a connection between the frequency of ARs and the joint phasing of AO and PNA. Specifically, increased AR frequency appears to be associated with the coexistence of −AO and −PNA. Consistent with that, ARs were quiescent or occurred much less frequently during other months of the season when such condition of the AO and PNA was generally not present. It is noted that considerable number of non-AR snow events did occur during February and March when PNA transitioned from negative to positive phase while AO mostly stayed in positive phase. Some of those non-AR snow events accumulated SWE comparable to ARs. It is likely that AR and non-AR events may have different relationships with the phasing of AO/PNA due to different synoptic features [*Warner et al.*, 2012], which is further examined below.

3.3. Modulation of Storm Frequency

[14] The climatological relationship between AR frequency in California and the phasing of AO and PNA is shown in Figure 6 (left). AR frequency is calculated as the percent AR days out of all days in a given AO or PNA phase during November–March, WY1998–2011. As seen, significantly increased AR frequency is associated with the negative phase of AO and PNA. The AR frequency increases by ∼90% between the positive and negative

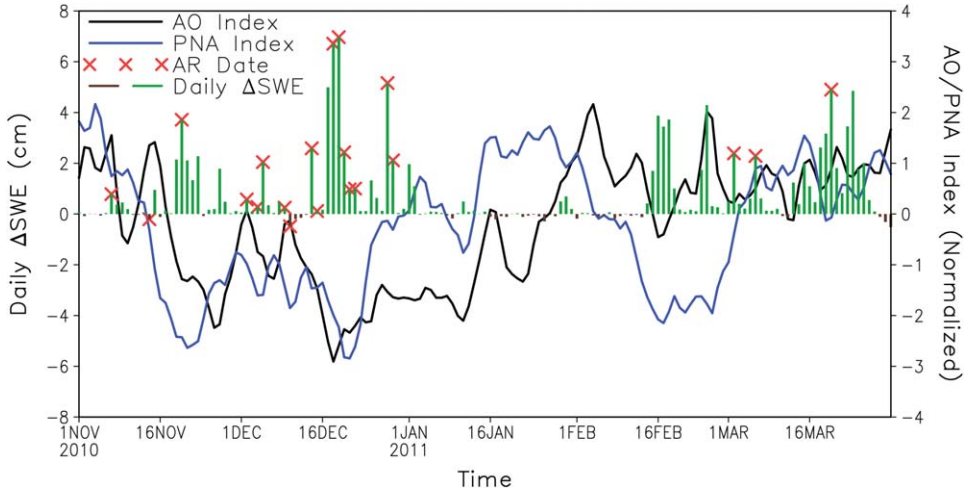

Figure 5. Mean daily ΔSWE (cm; green bars > 0 and brown bars < 0) over snow sensors in the Sierra Nevada, AO and PNA indices (black and blue traces, respectively), and AR dates (red "cross") during November 2010–March 2011. The AO and PNA indices are normalized by their respective standard deviations over the period of 1950–2011.

phases of AO, and by ~50% between the positive and negative phases of PNA. The increase in AR frequency is more dramatic (about a factor of four) between the days when AO and PNA are both in positive phase and when they are both in negative phase. Compared to the overall AR frequency when all winter days are considered (Figure 6, thick dashed line), AR frequency is more than doubled during the days when AO and PNA are both in negative phase. Similar analysis for non-AR wet days shows although their frequency is increased during the negative phase of AO and PNA (Figure 6, right), the magnitude of such increase is much smaller compared to the case of ARs.

[15] The magnitude and significance of the difference in AR frequency between joint −AO and −PNA versus +AO and +PNA motivates an examination of the dynamical nature of such a relationship. Typical circulation patterns associated with the negative phase of AO and PNA for WY1998–2011 are shown in Figures 7a and 7b in terms of the composite mean 500 hPa geopotential height anomalies. Both the −AO and −PNA have an associated low pressure system near the west coast of North America, but at distinctly different locations. The −AO low pressure is centered over the northeastern Pacific offshore California (Figure 7a), while the −PNA low pressure is centered

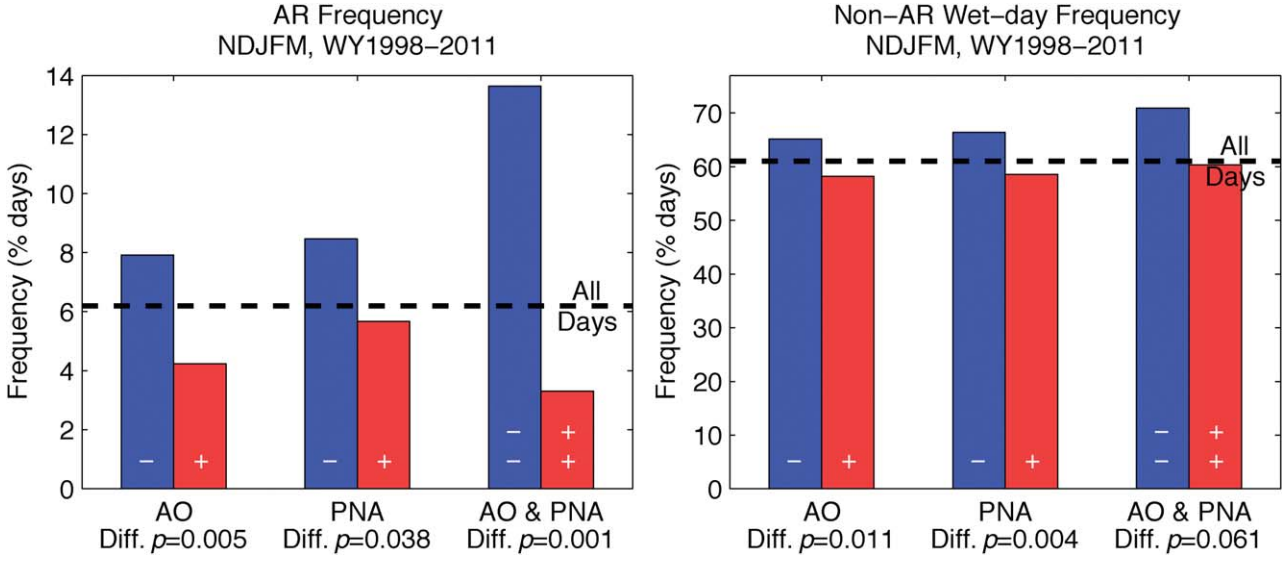

Figure 6. (left) AR frequency and (right) non-AR wet-day frequency (percent days) in California over negative (blue) and positive (red) phases of AO and PNA during the winter months (November–March) of WY1998–2011. The statistical significance (p value) of the difference between the blue and red bars in each set is indicated. The thick dashed line in each plot shows the AR frequency or non-AR wet-day frequency over all winter days. Negative/positive phases of AO and PNA are defined as the days when their respective index is 0.5 standard deviation below/above zero.

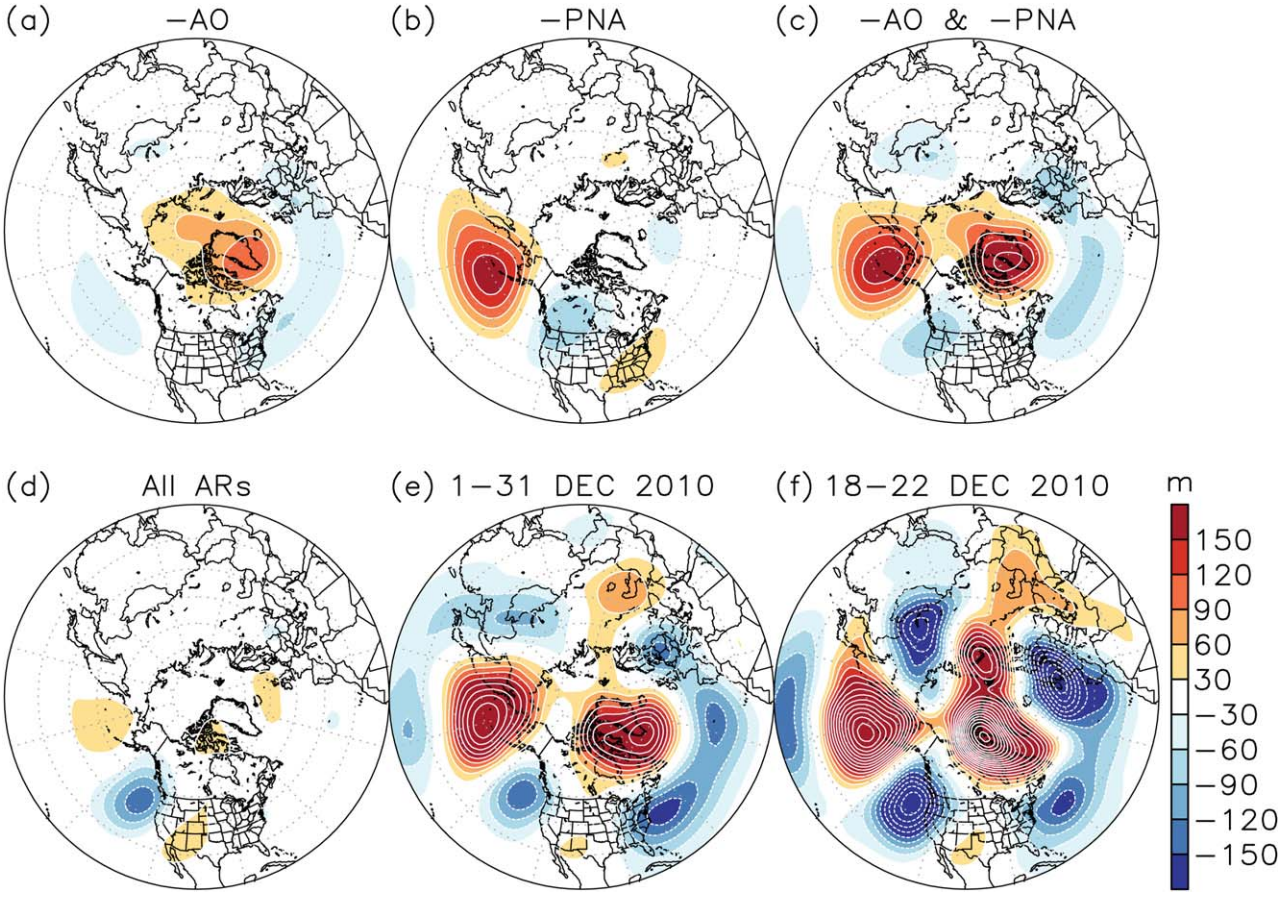

Figure 7. Mean 500 hPa geopotential height anomalies (m) averaged over the days when (a) the AO is in negative phase, (b) the PNA is in negative phase, (c) both the AO and the PNA are in negative phase during November–March, WY1998–2011, (d) ARs make landfall in California during November–March, WY1998–2011, and over (e) the month of December 2010 and (f) 18–22 December 2010. Anomalies are relative to the daily climatology over the period of WY1998–2011. The composites in Figures 7a–7c are based on days when the AO/PNA index is 0.5 standard deviation below zero.

overland northeast of California (Figure 7b). In both cases, onshore winds (i.e., blowing toward the Sierra Nevada) are implied over/near the southern two thirds of California. Compared to −AO and −PNA alone, their coexistence is characterized by a low pressure system more favorably situated for southwesterly winds blowing toward the Sierra Nevada (Figure 7c). In that regard, the two blocking highs in the Arctic and North Pacific, one apparently associated with the AO and the other with the PNA, may be of crucial importance to keep the associated low pressure system in place, which is shifted from its typical locations when only one of AO and PNA is active.

[16] Conceivably, the circulation pattern in Figure 7c provides a dynamical background favorable for the development of ARs that will ultimately impact California's Sierra Nevada. The low pressure system centered northwest of California is reminiscent of the mean circulation anomaly pattern when ARs make landfalls in California (Figure 7d). While not all ARs are associated with strong planetary-scale blocking patterns, as indicated by the lack of strength in the positive height anomalies in the AR composite (Figure 7d), the 14 ARs in December 2010 indeed occurred during a period of strong blocking in the Arctic and North Pacific (Figure 7e). The pattern of the circulation anomalies in that month is remarkably similar to the composite mean for coexisting −AO and −PNA (Figure 7c). The anomaly pattern during December 18–22, 2010 (Figure 7f), when five AR dates occurred in a row, also resembles that in Figure 7c.

3.4. Modulation of Storm Intensity

[17] The total seasonal SWE is affected by both the frequency of storms and the amount of snow accumulation during each storm. This section examines the possible influence of leading climate modes on daily ΔSWE during AR and non-AR dates. ENSO is considered in addition to AO and PNA given strong La Niña conditions in the 2010/2011 winter. Modulation of daily ΔSWE by these modes is calculated as the mean difference between negative and positive phases and done separately over AR and non-AR dates. The difference values are scaled by 0.5 to reflect the mean amplitude of modulation in each phase of the modes. For ARs, the largest modulation is by AO (Figure 8a), with the amplitude of modulation 23% of the mean AR daily ΔSWE (not shown). The amplitudes are relatively smaller for PNA and ENSO (Figures 8b and 8c), which are 6–10%

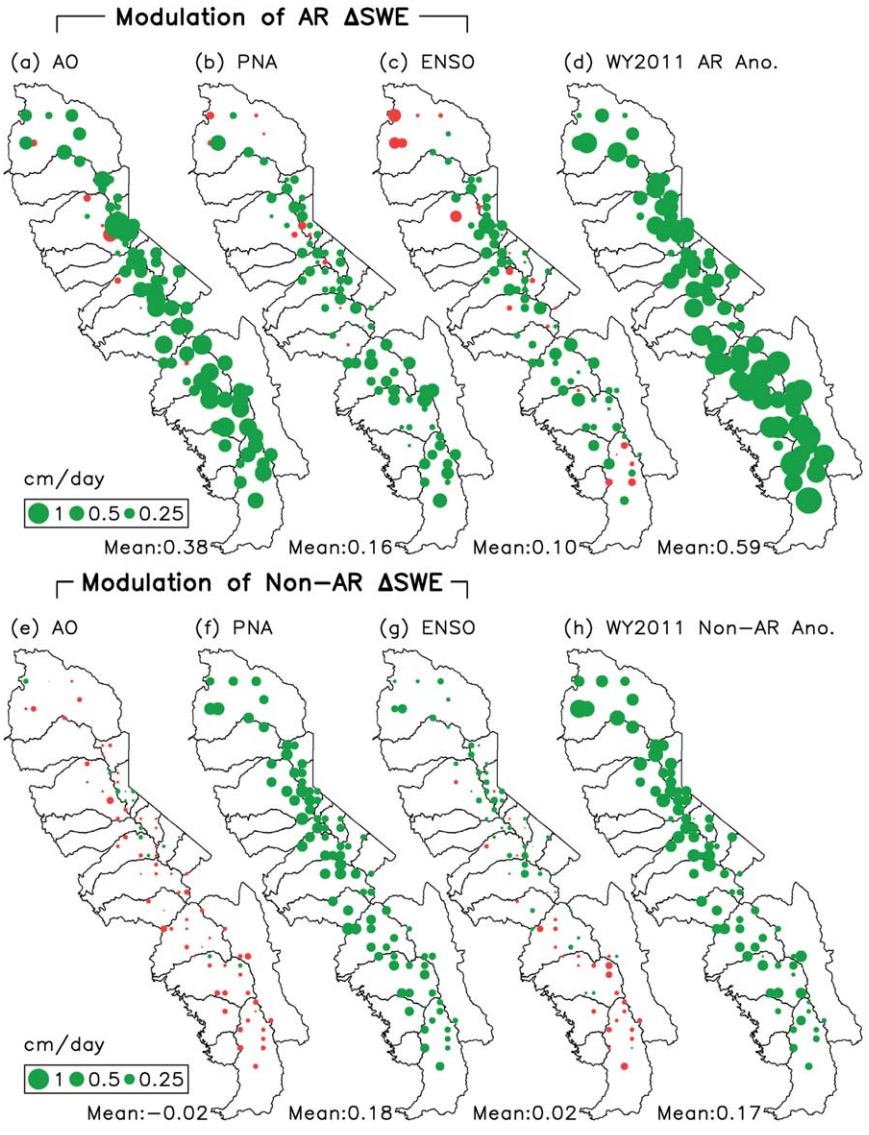

Figure 8. Mean difference in AR daily ΔSWE (cm) between negative and positive phases (the former minus the latter) of (a) AO, (b) PNA, and (c) ENSO during WY1998–2011; the signs represent the modulation during the negative phase, and the values have been scaled by 0.5 to reflect the amplitude of modulation. Positive numbers are in green, and negative values in red. (d) Mean daily ΔSWE (cm) over ARs during WY2011 relative to mean daily ΔSWE over all ARs during WY1998–2011. Only winter (November–March) ARs in California are considered. (e–h) As Figures 8a–8d but for non-AR wet days.

of the mean AR daily ΔSWE. The magnitude of the AR daily ΔSWE anomaly during the 2010/2011 winter (Figure 8d), which is 36% of the mean AR daily ΔSWE, is consistent with the combined magnitude of modulation by AO, PNA, and ENSO. For non-AR wet days, the modulation by the three modes are all small (Figures 8e–8g), which is consistent with the smallness of daily ΔSWE anomalies during non-AR wet days of the 2010/2011 winter (Figure 8h). Taken together, the analysis in sections 3.2–3.4 suggests the anomalous snow accumulation in the 2010/2011 winter is primarily associated with dramatically increased frequency of ARs, and to a lesser extent above-normal snow accumulation during these ARs, which is consistent with the magnitude of modulation on AR frequency and ΔSWE by the three leading climate modes considered.

[18] The physical processes underlying the relationship shown in Figures 8a–8d need to be understood. On one hand, AR precipitation is largely determined by the influx of water vapor [*Neiman et al*., 2009]. On the other hand, air temperature affects the partitioning between rain and snow hence SWE accumulation [*Guan et al*., 2010]. To understand the respective role of these processes, strengths of wintertime California ARs (in terms of IWV and IVT) and AR-related surface air temperature anomalies are compared between negative and positive phases of AO, PNA, and ENSO. Typical California ARs are characterized by an IWV tongue extending from the tropical/subtropical eastern Pacific to the California coast (Figure 9g). Associated IVT is directed in a focused band toward the Sierra Nevada. The IWV and IVT agree with each other in describing the AR

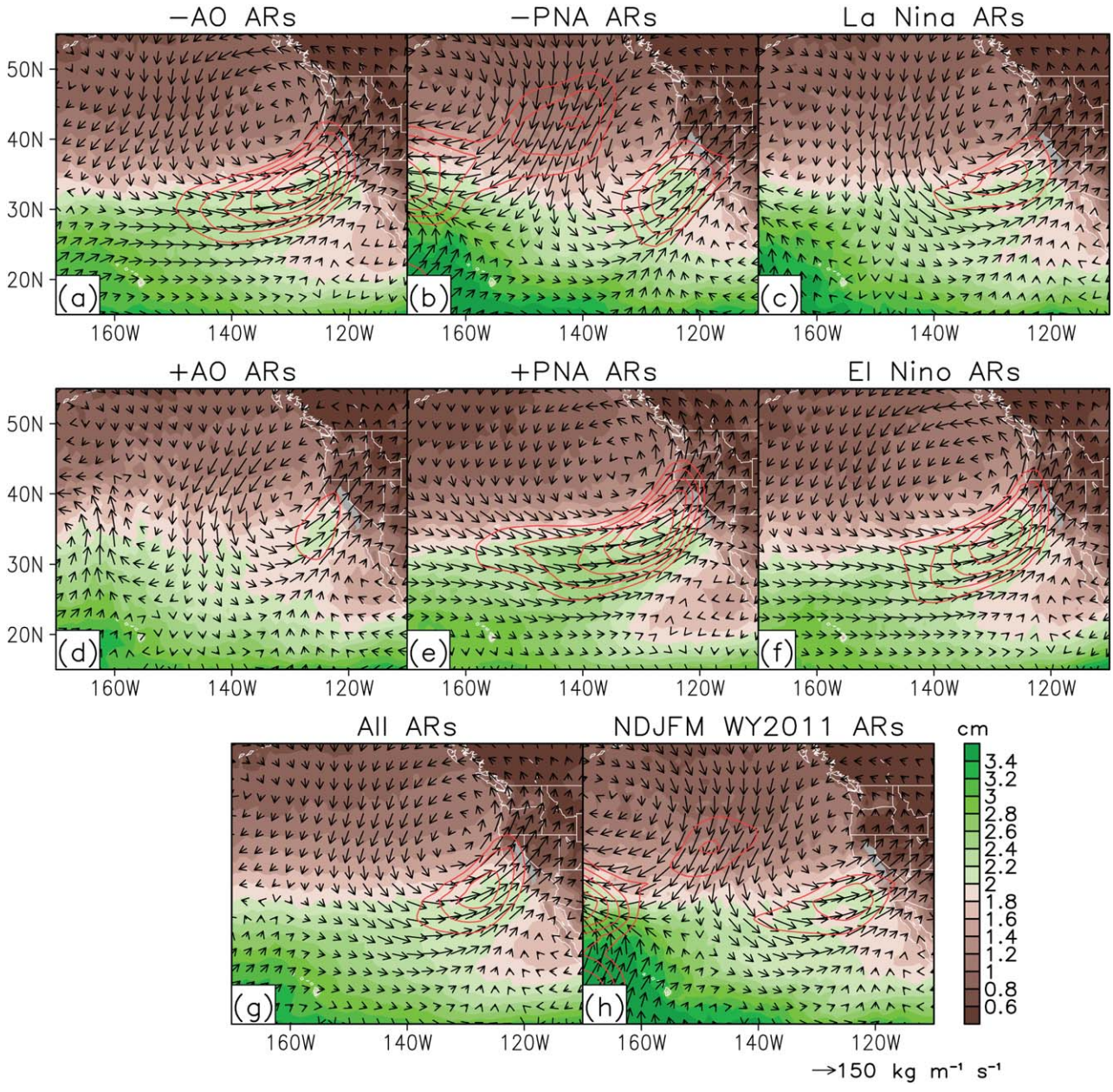

Figure 9. IWV values (cm; shading) and 1000–300 hPa IVT anomalies (kg m^{-1} s^{-1}; vectors) during California ARs averaged over negative and positive phases of (a and d) AO, (b and e) PNA, and (c and f) ENSO during WY1998–2011, (g) all ARs during WY1998–2011, and (h) ARs during WY2011. Only the winter months (November–March) are considered. Red contours show IVT magnitudes at 25 kg m^{-1} s^{-1} intervals, starting from 150 kg m^{-1} s^{-1}. Gray shading indicates the location of the Sierra Nevada. IWV is from AIRS satellite retrievals. IVT is from the NCEP/NCAR reanalysis.

location and orientation. The agreement is consistent with the basis for creating the record of landfalling ARs in *Neiman et al*. [2008], where satellite IWV was used as a proxy for IVT in AR detection. Mean strength of ARs is much larger during the negative phase of AO than during the positive phase in terms of IWV and IVT (Figures 9a and 9d). The contrary is true in the case of PNA (Figures 9b and 9e) and ENSO (Figures 9c and 9f), for which ARs are weaker during the negative phase. Compared to the mean of all ARs (Figure 9g), ARs are weaker during the 2010/2011 winter season (Figure 9h), consistent with compensating effects from AO, PNA, and ENSO. Increased daily ΔSWE during the 2010/2011 winter ARs is therefore not explained by the strengths of these ARs.

[19] Among the three modes, AO and ENSO have more coherent modulation on AR temperature, with surface air temperature on average 0.4°C colder than normal during their negative phase (Figures 10a and 10c). Modulation by PNA is weaker and with more mixed signs in the southern portion of the Sierra Nevada (Figure 10b). Previous studies have showed that AR storms are typically warmer (i.e., higher altitude of the freezing level) than other winter

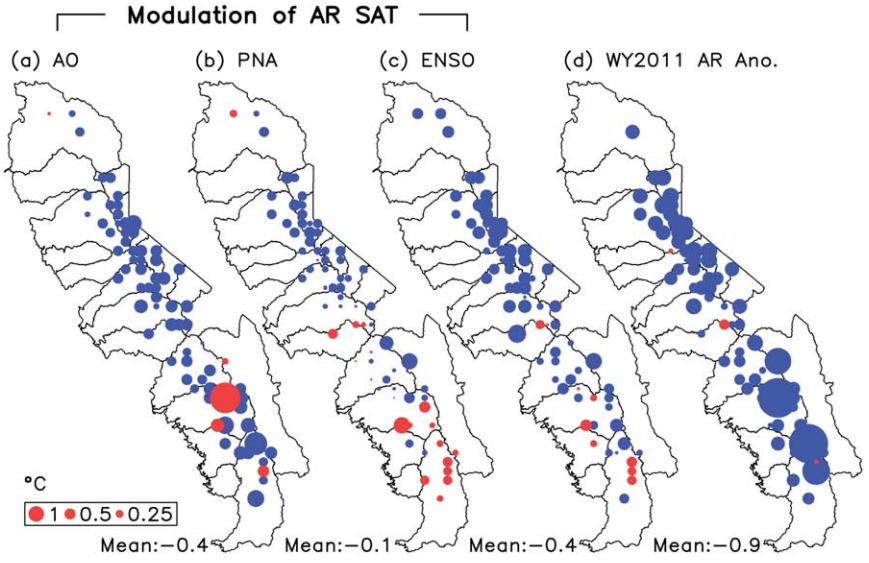

Figure 10. As Figures 8a–8d but for surface air temperature anomalies (°C). Positive numbers are in red, and negative values in blue. Note that the signs in Figures 10a–10c represent the modulation during the negative phase. Data are from daily temperature measurements at the snow sensor stations over WY2006–2011 (data before WY2006 are not used due to reduced spatial coverage).

storms [e.g., *Neiman et al*., 2008a, 2011; *Kim et al*., 2013; *Warner et al*., 2012] therefore more sensitive to small temperature variations in terms of snow-rain ratio [*Guan et al*., 2010]. ARs during the 2010/2011 winter are on average colder than normal ARs by 0.9°C (Figure 10d), which is favorable for snow accumulation despite that those ARs are on average weaker than normal in terms of water vapor transport.

4. Discussion

[20] The difference in SWE anomalies on 1 April 2011 evaluated with three products (Figure 2) highlights the challenge in accurately estimating SWE in topographically complex areas, especially over such large domains as the Sierra Nevada. Improvements in high spatial-resolution SWE products [e.g., *Durand et al*., 2008] will help better quantify the contribution of ARs to mountain snowpack and the impacts of ARs on watershed and subwatershed scales.

[21] It should be noted that the processing technique used to retrieve IWV changed starting in WY2009 due to changes in instrumentation from SSM/I to SSMIS. This change eliminated a pre-existing low bias in IWV which likely resulted in ARs being undetected prior to WY2009 with the exact degree of undercounting remaining to be quantified. As such, AR contribution to SWE prior to WY2009 could be higher than reported in Figure 3, and the relative magnitude of the 2010/2011 winter season in terms of AR frequency and AR-related SWE accumulation could be less pronounced than reported here. On the other hand, the relationships between ARs and the various climate variability modes examined are less likely to be affected by the potential undercounting in AR, unless such undercounting preferentially occurred during one phase of the modes than the other.

[22] The current analysis focused on the impact of AO, PNA, and ENSO on the frequency, strength, and snowpack impact of ARs in the Sierra Nevada, especially during the 2010/2011 winter season. Issues yet to be explored include the possible controls of these large-scale modes on the landfalling location of ARs, which may have critical impacts on AR precipitation and/or flooding depending on the topographic and geological characteristics of the river basins under impact [*Neiman et al*., 2011; *Lavers et al*., 2011, 2012]. For example, AR landfalls in the southern (northern) Europe were shown linked to the negative (positive) phase of the North Atlantic Oscillation—a close relative of the AO [*Lavers and Villarini*, 2013]. The more zonal direction of the low-level winds over the Pacific Northwest during the negative phase of PNA versus the more meridional winds during the positive phase may have different implications on AR landfalls in that area (M. D. Dettinger, personal communication, 2013).

[23] The connection between ARs and ENSO remain to be further investigated. *Dettinger* [2004] explored the possible linkages between AR-like features along the west coast of North America in over 50 years of NCEP/NCAR reanalysis data and the state of the ENSO and the Pacific Decadal Oscillation [PDO; *Mantua et al*., 1997], and suggested these features are most pronounced during warm PDO (i.e., El Niño-like) and neutral/near-neutral ENSO conditions. *Bao et al*. [2006] suggested a weakened subtropical Pacific high during the neutral phase of ENSO is the most favorable for the direct entrainment of tropical water vapor by ARs in the eastern Pacific, and a strengthened subtropical ridge during El Niño provides an unfavorable condition in that regard. The current analysis, on the other hand, indicates that ARs are stronger during El Niño than during La Niña conditions over the period of WY1998–2011. A systematic investigation of the AR-ENSO relationship will likely need to take into account the different types of ARs and/or ENSO itself. Some ARs appear to have a more direct entrainment of the tropical water vapor than others [*Neiman et al*., 2008b; *Ralph et al*.,

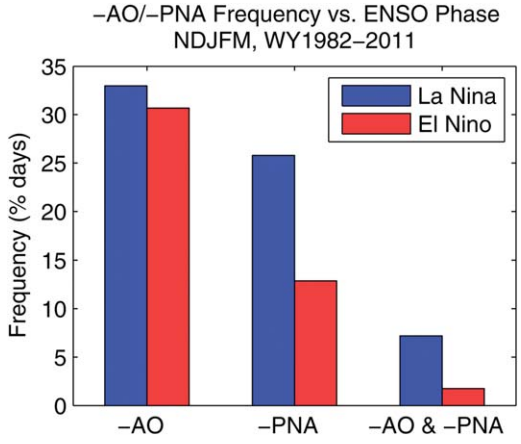

Figure 11. The frequency (% days) of −AO, −PNA, and joint −AO and −PNA days in a given ENSO phase.

2011; *Neiman et al*., 2013], and some have a water vapor source further west, stemming from the western Pacific [*Ralph and Dettinger*, 2011]. The characteristics of ENSO also change over time. Increased occurrence and intensity of central-Pacific El Niño events as opposed to the canonical eastern Pacific events have been observed during the recent few decades [*Lee and McPhaden*, 2010], with central-Pacific El Niño being the dominant type of events in the first decade of the 21st century [*Yu et al*., 2012]. An extended, more detailed record of AR landfalls that includes the time, location, and detailed structure of ARs [e.g., *Wick et al*., 2013], as well as improved understanding of the two types of ENSO, will facilitate a robust accounting of the impact of ENSO on ARs.

[24] Of the 20 AR dates during the 2010/2011 winter season, five are associated with MJO phase 6 (mean amplitude 0.9; based on the definition of *Wheeler and Hendon* [2004]) and five associated with phase 7 (mean amplitude 1.0), i.e., when the MJO convective signals are located in the western Pacific. Other MJO phases occurred less frequently during the 20 AR dates (between 0 and 4 times). In particular, the first four of the five consecutive AR dates during December 18–22, 2010 are accompanied by MJO convection in the western Pacific. This is consistent with *Guan et al*. [2012] who showed that among the eight MJO phases, phase 6 is the most favorable for high-impact AR landfalls in the Sierra Nevada based on data during WY1998–2010.

[25] The study focused on the snow accumulation period. Cold surface anomalies during the late snow season can suppress interstorm winter season snowmelt which would otherwise reduce total snowpack accumulation. Interestingly, both ENSO and the PDO were in their cold phase during the 2010/2011 winter season. Cold surface air temperature anomalies of 3–4 K were present throughout the Sierra Nevada during March 2011.

[26] It is noted that 20 joint −AO and −PNA days occurred in December 2010 (with 14 AR dates)—the highest monthly occurrence of such conditions during the AR record period (WY1998–2011). Monthly occurrence was between 0 and 12 during other months of the period. Therefore, December 2010 is unique during the 14 year analysis period both in terms of AR frequency and the occurrence of joint −AO and −PNA days. It is one of the 5 months after 1950 (March 1955, November 1965, January 1969, December 1996, and December 2010) during which the number of joint −AO and −PNA days exceeded 15. Although formal detection of ARs has not been performed for the period before WY1998 due to unavailability of high quality IWV observations, examination of the daily reanalysis IWV and IVT fields suggests that high frequency of ARs (on the order of 10 dates per month) occurred in California in four out of these five months. This connection between increased AR frequency and joint −AO and −PNA is consistent with the main analysis based on the AR record period.

[27] The close connections between AR frequency/characteristics and major modes of climate variability have implications on seasonal and longer-scale predictability of wintertime precipitation (extreme events, in particular) in California, which is especially important from a water resource perspective. ENSO predictions are routinely made by the Climate Prediction Center at seasonal lead times. On the other hand, forecast skills of seasonal AO and PNA variability are quite low [*Derome et al*., 2005]. It is of interest to note the factor of two differences in the frequency of −PNA days and the factor of four differences in the frequency of joint −AO and −PNA days between the two phases of ENSO (Figure 11), which have implications on potential predictability of seasonal AR activity in association with ENSO. Improved understanding and long-lead prediction of the AR-related modes of large-scale variability will help to better predict and manage regional water resources and floods.

5. Conclusions

[28] Mean SWE anomaly in California's Sierra Nevada on April 1, 2011 was 0.44 m (56%) above normal averaged over 100 snow sensors. November–March, WY2011 had the largest snow accumulation, largest number of ARs, and largest AR-related snow accumulation within the analysis period of WY1998–2011. A total of 20 AR dates occurred during the season, 14 of which were in December 2010, placing the season and the month on the top of the list in terms of AR frequency during the analysis period. The number of ARs in December 2010 is well above the normal range (i.e., 1.5 interquartile range above the third quartile), constituting a statistical outlier. Fifteen (14 in December and one in mid-November) out of the 20 AR dates during the season were associated with negative phase of AO and PNA. The five consecutive AR dates during December 18–22 were accompanied by particularly strong −AO and −PNA. Climatologically, AR frequency is increased during −AO and −PNA based on the analysis of all winter ARs in California during WY1998–2011. The increase from the positive to negative phases is by ∼90% for AO, and by ∼50% for PNA. The coexistence of −AO and −PNA creates a circulation pattern favorable for the development of ARs impacting California's Sierra Nevada and is characterized by cyclonic anomalies centered northwest of California. Such a teleconnection is consistent with the month of December 2010, when an exceptionally large number of ARs occurred during a period of persistently strong −AO and −PNA. Despite that the ARs of the 2010/2011 winter

are weaker than normal ARs in California in terms of water vapor transport, mean daily ΔSWE is 36% higher than normal, consistent with colder surface air temperatures during these ARs. The analysis suggests that the massive Sierra Nevada snowpack during the 2010/2011 winter season is primarily related to anomalously high frequency of ARs favored by the joint phasing of −AO and −PNA, and that a secondary contribution is from increased snow accumulation during these ARs favored by colder air temperatures associated with −AO, −PNA, and La Niña. The results highlight the importance of understanding the relationship between AR activity and the large-scale ocean-atmosphere variability for better prediction and management of water resources/floods in California and other western states.

[29] **Acknowledgments.** This research was supported by NASA grants NNX08AH18G and NNXIIAK35A, NSF grant EAR1032295, and by American Recovery and Reinvestment Act (ARRA) funds. Additional support was provided by the Water Resources Area of the NASA Applied Sciences Program. DEW's, EJF's, and BG's contribution, and part of NPM's contribution, to this study were carried out on behalf of the Jet Propulsion Laboratory, California Institute of Technology, under a contract with the National Aeronautics and Space Administration.

References

Bales, R. C., N. P. Molotch, T. H. Painter, M. D. Dettinger, R. Rice, and J. Dozier (2006), Mountain hydrology of the western United States, *Water Resour. Res.*, *42*, W08432, doi:10.1029/2005WR004387.

Bao, J.-W., S. A. Michelson, P. J. Neiman, F. M. Ralph, and J. M. Wilczak (2006), Interpretation of enhanced integrated water vapor bands associated with extratropical cyclones: Their formation and connection to tropical moisture, *Mon. Weather Rev.*, *134*, 1063–1080, doi:10.1175/MWR3123.1.

Carroll, T., D. Cline, G. Fall, A. Nilsson, L. Li, and A. Rost (2001), NOHRSC operations and the simulation of snow cover properties for the conterminous U.S., in Proceedings of the 69th Annual Meeting of the Western Snow Conference, pp. 1–14, Sun Valley, Idaho.

Cayan, D. R. (1996), Interannual climate variability and snowpack in the western United States, *J. Clim.*, *9*, 928–948, doi:10.1175/1520-0442(1996)009<0928:ICVASI>2.0.CO;2.

Chahine, M. T., et al. (2006), AIRS: Improving weather forecasting and providing new data on greenhouse gases, *Bull. Am. Meteorol. Soc.*, *87*, 911–926.

Derome, J., H. Lin, and G. Brunet (2005), Seasonal forecasting with a simple general circulation model: Predictive skill in the AO and PNA, *J. Clim.*, *18*, 597–609, doi:10.1175/JCLI-3289.1.

Dettinger, M. D. (2004), Fifty-two years of "pineapple-express" storms across the west coast of North America, PIER Energy-Related Environ. Res. Rep. CEC-500–2005-004, 15 pp., U.S. Geol. Surv., Scripps Inst. of Oceanogr. for the Calif. Energy Com., La Jolla, California. [Available at http://www.energy.ca.gov/2005publications/CEC-500–2005-004/CEC-500–2005-004.pdf.]

Dettinger, M. D., F. M. Ralph, T. Das, P. J. Neiman, and D. R. Cayan (2011), Atmospheric rivers, floods, and the water resources of California, *Water*, *3*, 445–478, doi:10.3390/w3020445.

Durand, M., N. P. Molotch, and S. A. Margulis (2008), A Bayesian approach to snow water equivalent reconstruction, *J. Geophys. Res.*, *113*, D20117, doi:10.1029/2008JD009894.

Guan, B., N. P. Molotch, D. E. Waliser, E. J. Fetzer, and P. J. Neiman (2010), Extreme snowfall events linked to atmospheric rivers and surface air temperature via satellite measurements, *Geophys. Res. Lett.*, *37*, L20401, doi:10.1029/2010GL044696.

Guan, B., D. E. Waliser, N. P. Molotch, E. J. Fetzer, and P. J. Neiman (2012), Does the Madden-Julian Oscillation influence wintertime atmospheric rivers and snowpack in the Sierra Nevada? *Mon. Weather Rev.*, *140*, 325–342, doi:10.1175/MWR-D-11–00087.1.

Guan, B., N. P. Molotch, D. E. Waliser, S. M. Jepsen, T. H. Painter, and J. Dozier (2013), Snow water equivalent in the Sierra Nevada: Blending snow sensor observations with snowmelt model simulations, *Water Resour. Res.*, *49*, 5029–5046, doi:10.1002/wrcr.20387.

Hollinger, J. P., J. L. Peirce, and G. A. Poe (1990), SSM/I instrument evaluation, *IEEE Trans. Geosci. Remote Sens.*, *28*, 781–790.

Jeong, J.-H., and C.-H. Ho (2005), Changes in occurrence of cold surges over east Asia in association with Arctic Oscillation, *Geophys. Res. Lett.*, *32*, L14704, doi:10.1029/2005GL023024.

Jepsen, S. M., N. P. Molotch, M. W. Williams, K. E. Rittger, and J. O. Sickman (2012), Interannual variability of snowmelt in the Sierra Nevada and Rocky Mountains, USA: Examples from two alpine watersheds, *Water Resour. Res.*, *48*, W02529, doi:10.1029/2011WR011006.

Jiang, T., and Y. Deng (2011), Downstream modulation of North Pacific atmospheric river activity by East Asian cold surges, *Geophys. Res. Lett.*, *38*, L20807, doi:10.1029/2011GL049462.

Kalnay, E., et al. (1996), The NCEP/NCAR 40-Year Reanalysis Project, *Bull. Am. Meteorol. Soc.*, *77*, 437–471.

Kapnick, S., and A. Hall (2010), Observed climate–snowpack relationships in California and their implications for the future, *J. Clim.*, *23*, 3446–3456, doi:10.1175/2010JCLI2903.1.

Kim, J., D. E. Waliser, P. J. Neiman, B. Guan, J.-M. Ryoo, and G. A. Wick (2013), Effects of atmospheric river landfalls on the cold season precipitation in California, *Clim. Dyn.*, *40*(1–2), 465–474, doi:10.1007/s00382-012-1322-3.

Lavers, D. A., and G. Villarini (2013), The nexus between atmospheric rivers and extreme precipitation across Europe, *Geophys. Res. Lett.*, *40*, 3259–3264, doi:10.1002/grl.50636.

Lavers, D. A., R. P. Allan, E. F. Wood, G. Villarini, D. J. Brayshaw, and A. J. Wade (2011), Winter floods in Britain are connected to atmospheric rivers, *Geophys. Res. Lett.*, *38*, L23803, doi:10.1029/2011GL049783.

Lavers, D. A., G. Villarini, R. P. Allan, E. F. Wood, and A. J. Wade (2012), The detection of atmospheric rivers in atmospheric reanalyses and their links to British winter floods and the large-scale climatic circulation, *J. Geophys. Res.*, *117*, D20106, doi:10.1029/2012JD018027.

Lee, T., and M. J. McPhaden (2010), Increasing intensity of El Niño in the central-equatorial Pacific, *Geophys. Res. Lett.*, *37*, L14603, doi:10.1029/2010GL044007.

Leung, L. R., and Y. Qian (2009), Atmospheric rivers induced heavy precipitation and flooding in the western U.S. simulated by the WRF regional climate model, *Geophys. Res. Lett.*, *36*, L03820, doi:10.1029/2008GL036445.

Mantua, N. J., S. R. Hare, Y. Zhang, J. M. Wallace, and R. C. Francis (1997), A Pacific interdecadal climate oscillation with impacts on salmon production, *Bull. Am. Meteorol. Soc.*, *78*, 1069–1079, doi:10.1175/1520-0477(1997)078<1069:APICOW>2.0.CO;2.

McAfee, S. A., and J. L. Russell (2008), Northern Annular Mode impact on spring climate in the western United States, *Geophys. Res. Lett.*, *35*, L17701, doi:10.1029/2008GL034828.

Molotch, N. P. (2009), Reconstructing snow water equivalent in the Rio Grande headwaters using remotely sensed snow cover data and a spatially distributed snowmelt model, *Hydrol. Processes*, *23*, 1076–1089, doi:10.1002/hyp.7206.

Molotch, N. P., and R. C. Bales (2005), Scaling snow observations from the point to the grid-element: Implications for observation network design, *Water Resour. Res.*, *41*, W11421, doi:10.1029/2005WR004229.

Molotch, N. P., and R. C. Bales (2006), SNOTEL representativeness in the Rio Grande headwaters on the basis of physiographics and remotely sensed snow cover persistence, *Hydrol. Processes*, *20*, 723–739, doi:10.1002/hyp.6128.

Moore, B. J., P. J. Neiman, F. M. Ralph, and F. E. Barthold (2012), Physical processes associated with heavy flooding rainfall in Nashville, Tennessee, and vicinity during 1–2 May 2010: The role of an atmospheric river and mesoscale convective systems, *Mon. Weather Rev.*, *140*, 358–378, doi:10.1175/MWR-D-11–00126.1.

National Operational Hydrologic Remote Sensing Center (2004), Snow Data Assimilation System (SNODAS) data products at NSIDC, November 2003–March 2010, Natl. Snow and Ice Data Cent., Boulder, Colo. [Available at http://nsidc.org/data/docs/noaa/g02158_snodas_snow_cover_model/index.html.]

Neiman, P. J., F. M. Ralph, G. A. Wick, J. D. Lundquist, and M. D. Dettinger (2008a), Meteorological characteristics and overland precipitation impacts of atmospheric rivers affecting the West Coast of North America based on eight years of SSM/I satellite observations, *J. Hydrometeorol.*, *9*, 22–47, doi:10.1175/2007JHM855.1.

Neiman, P. J., F. M. Ralph, G. A. Wick, Y.-H. Kuo, T.-K. Wee, Z. Ma, G. H. Taylor, and M. D. Dettinger (2008b), Diagnosis of an intense atmospheric river impacting the Pacific Northwest: Storm summary and offshore vertical structure observed with COSMIC satellite retrievals, *Mon. Weather Rev.*, *136*, 4398–4420, doi:10.1175/2008MWR2550.1.

Neiman, P. J., A. B. White, F. M. Ralph, D. J. Gottas, S. I. Gutman (2009), A water vapor flux tool for precipitation forecasting, *Water Manage.*, *162*, 83–94, doi:10.1680/wama.2009.162.2.83.

Neiman, P. J., L. J. Schick, F. M. Ralph, M. Hughes, and G. A. Wick (2011), Flooding in western Washington: The connection to atmospheric rivers, *J. Hydrometeorol.*, *12*, 1337–1358, doi:10.1175/2011JHM1358.1.

Neiman, P. J., F. M. Ralph, B. J. Moore, M. Hughes, K. M. Mahoney, J. Cordeira, and M. D. Dettinger (2013), The landfall and inland penetration of a flood-producing atmospheric river in Arizona. Part 1: Observed synoptic-scale, orographic, and hydrometeorological characteristics, *J. Hydrometeorol.*, *14*, 460– 484, doi:10.1175/JHM-D-12–0101.1.

Ralph, F. M., and M. D. Dettinger (2011), Storms, floods, and the science of atmospheric rivers, *Eos Trans. AGU*, *92*, 265, doi:10.1029/2011EO320001.

Ralph, F. M., and M. D. Dettinger (2012), Historical and national perspectives on extreme West Coast precipitation associated with atmospheric rivers during December 2010, *Bull. Am. Meteorol. Soc.*, *93*, 783–790, doi:10.1175/BAMS-D-11-00188.1.

Ralph, F. M., P. J. Neiman, and G. A. Wick (2004), Satellite and CALJET aircraft observations of atmospheric rivers over the eastern North Pacific Ocean during the winter of 1997/98, *Mon. Weather Rev.*, *132*, 1721–1745.

Ralph, F. M., P. J. Neiman, and R. Rotunno (2005), Dropsonde observations in low-level jets over the northeastern Pacific Ocean from CALJET-1998 and PACJET-2001: Mean vertical-profile and atmospheric-river characteristics, *Mon. Weather Rev.*, *133*, 889–910, doi:10.1175/MWR2896.1.

Ralph, F. M., P. J. Neiman, G. A. Wick, S. I. Gutman, M. D. Dettinger, D. R. Cayan, and A. B. White (2006), Flooding on California's Russian River: Role of atmospheric rivers, *Geophys. Res. Lett.*, *33*, L13801, doi:10.1029/2006GL026689.

Ralph, F. M., P. J. Neiman, G. N. Kiladis, K. Weickmann, and D. W. Reynolds (2011), A multiscale observational case study of a Pacific atmospheric river exhibiting tropical–extratropical connections and a mesoscale frontal Wave, *Mon. Weather Rev.*, *139*, 1169–1189, doi:10.1175/2010MWR3596.1.

Reynolds, R. W., T. M. Smith, C. Liu, D. B. Chelton, K. S. Casey, and M. G. Schlax (2007), Daily high-resolution-blended analyses for sea surface temperature, *J. Clim.*, *20*, 5473–5496, doi:10.1175/2007JCLI1824.1.

Thompson, D. W. J., and J. M. Wallace (1998), The Arctic oscillation signature in the wintertime geopotential height and temperature fields, *Geophys. Res. Lett.*, *25*, 1297–1300, doi:10.1029/98GL00950.

Trenberth, K. E. (1997), The definition of El Niño, *Bull. Am. Meteorol. Soc.*, *78*, 2771–2777, doi:10.1175/1520-0477(1997)078<2771:TDOENO>2.0.CO;2.

Trujillo, E., N. P. Molotch, M. L. Goulden, A. E. Kelly, and R. C. Bales (2012), Elevation-dependent influence of snow accumulation on forest greening, *Nat. Geosci.*, *5*, 705–709, doi:10.1038/ngeo1571.

Waliser, D. E., et al. (2011), Simulating cold season snowpack: Impacts of snow albedo and multi-layer snow physics, *Clim. Change*, *109*, 95–117, doi:10.1007/s10584-011-0312-5.

Waliser, D. E., B. Guan, J.-L. Li, and J. Kim (2012), Addendum to ''Simulating cold season snowpack: Impacts of snow albedo and multi-layer snow physics'': Waliser, D., J. Kim, Y. Xue, Y. Chao, A. Eldering, R. Fovell, A. Hall, Q. Li, K. N. Liou, J. McWilliams, S. Kapnick, R. Vasic, F. De Sale, and Y. Yu (2011), Climatic Change, 109 (Suppl 1):S95–S117, DOI 10.1007/s10584-011-0312-5, *Clim. Change*, *114*, 399–400, doi:10.1007/s10584-012-0531-4.

Wallace, J. M., and D. S. Gutzler (1981), Teleconnections in the geopotential height field during the Northern Hemisphere winter, *Mon. Weather Rev.*, *109*, 784–812.

Warner, M. D., C. F. Mass, and E. P. Salathé (2012), Wintertime extreme precipitation events along the Pacific Northwest coast: Climatology and synoptic evolution, *Mon. Weather Rev.*, *140*, 2021–2043, doi:10.1175/MWR-D-11–00197.1.

Wheeler, M. C., and H. H. Hendon (2004), An all-season real-time multivariate MJO index: Development of an index for monitoring and prediction, *Mon. Weather Rev.*, *132*, 1917–1932, doi:10.1175/1520-0493(2004)132<1917:AARMMI>2.0.CO;2.

Wick, G., P. J. Neiman, and F. M. Ralph (2013), Description and validation of an automated objective technique for identification and characterization of the integrated water vapor signature of atmospheric rivers, *IEEE Trans. Geosci. Remote Sens.*, *51*, 2166–2176, doi:10.1109/TGRS.2012.2211024.

Yu, J.-Y., Y. Zou, S. T. Kim, and T. Lee (2012), The changing impact of El Niño on US winter temperatures, *Geophys. Res. Lett.*, *39*, L15702, doi:10.1029/2012GL052483.

Zhu, Y., and R. E. Newell (1994), Atmospheric rivers and bombs, *Geophys. Res. Lett.*, *21*, 1999–2002, doi:10.1029/94GL01710.

Zhu, Y., and R. E. Newell (1998), A Proposed algorithm for moisture fluxes from atmospheric rivers, *Mon. Weather Rev.*, *126*, 725–735, doi:10.1175/1520-0493(1998)126<0725:APAFMF>2.0.CO;2.